On the generation mechanisms of fluid-driven seismic signals related to volcano-tectonics

Marco Fazio[1] (ID)**, Philip M. Benson[1]** (ID)**, and Sergio Vinciguerra[2]** (ID)

[1]Rock Mechanics Laboratory, University of Portsmouth, Portsmouth, UK, [2]Department of Earth Sciences, University of Turin, Turin, Italy

Abstract The generation mechanics of fluid-driven volcano seismic signals, and their evolution with time, remains poorly understood. We present a laboratory study aiming to better constrain the time evolution of such signals across temperature conditions 25 to 175°C in order to simulate a "bubbly liquid." Simulations used pressures equivalent to volcanic edifices up to 1.6 km in depth using a triaxial deformation apparatus equipped with an array of acoustic emission sensors. We investigate the origin of fluid-driven seismic signals by rapidly venting the pore pressure through a characterized damage zone. During the release of water at 25°C broadband signals were generated, with frequencies ranging from 50 to 160 kHz. However, the decompression of a water/steam phase at 175°C generated a bimodal spectrum of different signals, in the range 100–160 kHz. These new results are consistent with natural signals from active volcanoes, such as Mount Etna, and highlight the role of fluid and gas phases (such as bubbly liquids) in generating different types of volcano-tectonic seismicity.

1. Introduction

Seismicity is the short-term precursory phenomenon most frequently detected before volcanic unrest, occurring as the Earth's crust is fractured as magma moves its way to the surface and as fluids move within the faulted rock. Although different local terminologies have been widely used in the past [e.g., *McNutt*, 1996; *Chouet*, 1996; *Neuberg*, 2000; *McNutt*, 2005], according to *Chouet* [1996], volcano seismicity is defined in general terms of signal frequency or period.

Low-frequency (LF), also known as long-period (LP), events are characterized by a low harmonic frequency (0.5–5 Hz) [*Alparone et al.*, 2010] waveform lasting several seconds and a highly emergent onset that is difficult to identify. In contrast, high-frequency events generated by deformation/failure mechanisms within the volcanic edifice are generally recorded in the frequency range of up to 15 Hz, termed volcano-tectonic (VT) events, and feature an impulsive onset, a short broadband coda and higher energies. Between these two end-members, the so-called hybrid events share features from both VT activity and LF activity: an impulsive onset followed by a lower frequency coda. Volcanic tremor shows similar frequency content with respect to LP, but in a quasi-continuous signal that can last from minutes to months. Finally, very low frequency (VLF, 0.3–0.01 Hz), also known as very long period (VLP), events have also been recorded since the deployment of broadband instruments in the 1990s [*McNutt*, 2005]. These signals share the harmonic behavior of LPs and tremor, but at lower frequency.

The similarities between VLF, LF, and tremor suggest a common source process. For this reason, seismic signals may be grouped into (1) VLF, LF, and tremor likely generated as the result of fluid movement in fluid-filled cracks and (2) VT events originated from shear/tensile mechanisms occurring in the solid rock. Crucially from a hazard and risk perspective, the interplay between VLF, LF, tremor, and VT signals is diagnostic for understanding the fundamental magmatic processes within the volcanic structure and in particular to the pressurization of the volcanic plumbing system [e.g., *Chouet and Matoza*, 2013]. However, while great progress linking the underpinning geophysics to the families of seismic activity has been made over the past 20 years [e.g., *Chouet*, 1996, 2003; *McNutt*, 2005; *Chouet and Matoza*, 2013], the physical source of tremor, LF, and VLF events remains controversial. In particular, our knowledge of fluid/gas flow (decompression) rates needed to generate such signals and the coupling between different phases with respect to two-phase fluids such as "bubbly liquids" [e.g., *Kumagai and Chouet*, 2001] is lacking.

A key link is the causal relationship between LF events and tremor [*Neuberg*, 2000; *Saccorotti et al.*, 2007]. *Neuberg* [2000] found that individual LF events at Soufrière Hills volcano (Montserrat) were linked to

small-size, repetitive, nondestructive source areas which then merged into tremor before lava dome collapses. Later work by *Saccorotti et al.* [2007] distinguished two different seismic signals (LP and VLP) at Mount Etna volcano (Italy) during noneruptive periods and interpreted the shallow plumbing system in terms of the resonance of a fluid-filled buried cavity. However, as these processes cannot be directly observed, numerous models have been developed, often considering a fluid moving through a crack/damage network. In such an approach, the rapid fluid flow generates resonance within the crack [*Julian*, 1994], which is detected as a seismic event [e.g., *Chouet*, 1996, 2003]. Other generation mechanisms for the measured seismicity include brittle failure of magma at its glass transition point [*Tuffen and Dingwell*, 2005; *Neuberg et al.*, 2006] and "stick slip" during the extrusion of solidifying lava [*Iverson et al.*, 2006; *Kendrick et al.*, 2014]. Of these, the fluid-filled crack model is the most common [*Chouet and Matoza*, 2013], where LF events are generally viewed as the response of the system to a sudden transitory pressure or fluid flow event, while tremor is generated by supported pressure fluctuations [*Chouet*, 1996]. Assuming that the fluid is actively involved, the occurrence of low-frequency seismicity is considered to be a sign of pressurization in a magmatic/hydrothermal system, generating LF seismic activity that is, in turn, related to the rate and magnitude of pressurization and to the intensity of explosive activity [*Chouet*, 1996].

In this study we investigate the change in microseismic signal frequency as it evolves from tremor to LF by releasing high-pressure, high-temperature fluid (water) from a prefaulted sample of basalt from Mount Etna, recording the induced seismicity via acoustic emission (AE) analysis [e.g., *Burlini et al.*, 2007]. This is the laboratory analogue for field-scale seismicity and is widely used in rock physics experiments [e.g., *Benson et al.*, 2007, 2010]. While the vast majority of AE studies have focused on the nucleation and propagation of shear faulting analogous to VT and due to rupture processes that precede and accompany the formation of a major damage zone in a centimeter-scale rock specimen [e.g., *Ohnaka and Mogi*, 1982; *Read et al.*, 1995; *Benson et al.*, 2007], a more limited data set is available for the fluid-induced seismicity [e.g., *Burlini et al.*, 2007; *Benson et al.*, 2008, 2010, 2014]. In particular, these early studies of fluid (water)-induced AE have concentrated to date on water at ambient temperature conditions. Here we report new data taken from a more systematic study in order to better understand the subtle links between fluid phase on the character (frequency) of generated AE, linking these data to the statistics of the events in time and space. This is important, as the laboratory calibrations of these subtle effects are crucial for quantitative interpretation of field-scale data.

The key advantage of performing laboratory experiments is that conditions of pressure and temperature at which AE events occur are known and well controlled. Although real volcanic conditions act on different time and space scales and are different in terms of heterogeneity, the use of laboratory rock physics as a proxy for the microseismic source has shown to be a useful tool in reproducing the fundamental processes and the corresponding geophysical signatures at controlled stress conditions [e.g., *Read et al.*, 1995; *Sammonds*, 1999; *Burlini et al.*, 2007; *Benson et al.*, 2008]. It is also well established that the physical processes generating the laboratory AEs and those responsible for the volcanic earthquake are similar and scalable [e.g., *Aki and Richards*, 1980; *Burlini et al.*, 2007; *Benson et al.*, 2010]. Appropriate scaling approaches for centimeter-scale rock samples to a kilometer-scale volcanic edifice continue to be debated; however, basic qualitative interpretations can be made by considering similarities between laboratory and field waveforms/spectra and quantitatively by taking the size-frequency relationship [*Burlini et al.*, 2007; *Benson et al.*, 2010]. We hereafter report a suite of new experiments where we generated and analyzed seismic signals during the decompression of single- and dual-phase fluids under controlled temperature and confining pressure conditions.

2. Material Investigated and Experimental Procedures

The sample material was an alkali, porphyritic basalt from Mount Etna (Italy) with density $2870 \pm 10 \, \text{kg/m}^3$ and porosity $2.02 \pm 0.12\%$. Cylindrical samples of 100 mm (length) by 40 mm (diameter) were drilled using a standard diamond tipped coring drill. In addition, a conduit of 3 mm is drilled through the center of the long axis to enable pore fluid (water) to access the eventual damage zone. Experiments were carried out using an externally heated, servo-controlled triaxial apparatus (Figure S1 in the supporting information) at a confining pressure of 46 MPa and pore pressure of 16 MPa, yielding an effective pressure of 30 MPa and broadly representative of volcanic conditions and shallow plumbing systems at approximately 1.6 km depth. Standard triaxial deformation experiments were performed at a constant strain rate of $10^{-5} \, \text{s}^{-1}$, in order to generate

a shear/damage zone oriented at approximately 30° with respect to the loading. Once this shear zone and the associated damage zone are created, the maximum principal stress is then reduced to yield a hydrostatic stress condition (and therefore lock the fault). At this stage one of two protocols is followed, either (i) the external furnace increases sample temperature (and pore fluid temperature to 175°C) or (ii) the temperature is held constant at approximately 25°C. After this, in both cases, through a fast-acting solenoid valve connected to the lower end of the sample, the pore fluid pressure is rapidly released to the atmosphere via the rapid fluid flow from the established damage zone.

An array of 12 piezoelectric lead zirconate titanate sensors (six at 1 MHz central frequency and six at 200 kHz), embedded within an engineered Nitrile jacket [*Sammonds*, 1999], is used to compute *P* wave elastic velocities. This consists of "pulsing" sensors in sequence, with the remaining sensors recording the arrival of the signal via the time-of-flight method [*Pettitt*, 1998] and to derive a velocity model necessary for the location algorithm. A downhill simplex method [*Nelder and Mead*, 1965; *Press et al.*, 1994] is used to locate the microseismic (AE) events, extracted from the continuous signal, (which we term *streaming data*) recorded by 8 of the 12 channels. The streaming data are processed offline after the experiment allowing events to be "harvested" from this streamed waveform. Before being recorded, all signals are preamplified by dual 30 dB buffered amplifiers, which also incorporate a band-pass filter 10 kHz to 1 MHz to remove local noise. In this study, the use of lower frequency sensors allows for a more robust statistics when analyzing the fluid-induced (LF) AE data.

During the experiment, axial stress and pore fluid pressures are recorded via high-speed data acquisition systems. This enables the character and the frequency of the AE to be compared to the axial stress/pore pressure change, as a function of time.

3. Results

A series of seven experiments were performed (here shown the experiments with the best signal-to-noise ratio, SNR), with peak stress at failure measured between 436 and 465 MPa. After failure, a stress drop of approximately 250 MPa is measured (Figure S2), with posttest inspection revealing the classic shear fracture at 30° to the σ_1 direction. This part of the experiment generates a shear fault accessed by the central conduit. An instantaneous pore pressure release (hereafter called "venting") is then performed by discharging the pore fluid from the bottom of the sample via a solenoid valve and recording the pore pressures at high data acquisition rates of 5 kHz.

We find that the pore pressure decay follows a different path depending on sample temperature (Figure 1). At 25°C (experiment EB25) the lower pore pressure decreases instantaneously to zero (Figure 1a, solid green line), as it is directly connected to the solenoid valve. Meanwhile, the top pore pressure decays over a period of 2 min (Figure 1a, solid black line). At elevated temperatures of 175°C (experiment EB175), both bottom and top pressures decay quickly to approximately 1.5 MPa (Figure 1b, solid lines), followed by a more gentle decrease to 0.9 MPa over the following 10 s. Both pressures stabilize at this value over a period of 70 s, after which the bottom pore pressure decreases to 0.2 MPa. During the 2 min after the venting, the maximum cumulative AE hits (AE counts above a fixed threshold) occur during the main venting stage (around 1350 and 1500 cumulative hits in the first second in EB25 and EB175, respectively, Figures 1a and 1b, dashed red lines). At 25°C, 10 s after the release, the cumulative hits sharply increase up to a value of 1800 hits, while in the following 110 s cumulative AE hits increase at a slower rate reaching a total of 1900 at 120 s (Figure 1a). At 175°C a similar behavior is seen: after the initial peak, the cumulative hit rate steadily increased up to 1800 hits (Figure 1b).

Figure 1 shows a 58 ms segment around the initial pore pressure decay (Figures 1c and 1d, thick black and green lines), for both the raw streaming data waveform (Figures 1c and 1d, thin blue lines) and its frequency-power spectrogram (Figures 1e and 1f) of that AE activity as a function of time during venting. In EB25, the onset of a tremor-like AE activity occurred 12 ms after the release, with a duration of 10 ms (Figure 1c). Conversely, in EB175 the AE activity started 4 ms after the release. This AE tremor had a much longer duration (30 ms) than the tremor generated in EB25. In terms of frequency, for experiment EB25 we measured a broadband tremor with frequency ranging from 40 kHz to 200 kHz (Figure 1e), whereas for experiment EB175 a continuous spectrum was measured instead with frequency ranging between 100 kHz and 160 kHz (Figure 1f).
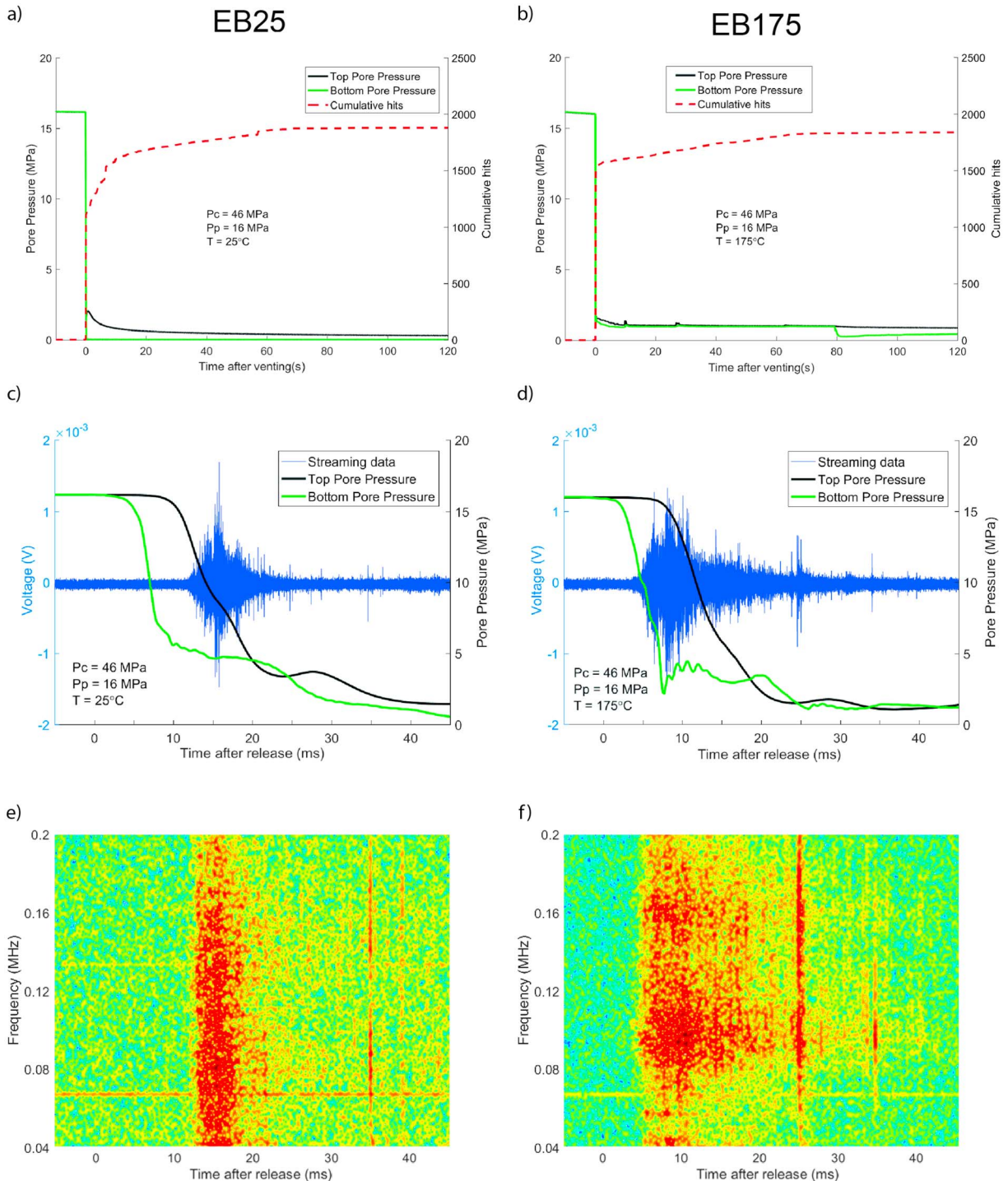
Figure 1. Venting stage for (a) EB25 and (b) EB175. Top (black) and bottom (green) pore pressure-time plot (left hand axis, solid lines) and cumulative hit rate (right-hand axis, dashed red line). In EB25 (Figure 1a) the top pore pressure decays quickly immediately after the release allowing further hits in the following 10 s, while fewer hits were recorded when the decrease was slower than the first part of the decay curve. In EB175, top and bottom pore pressures both stabilized at 0.9 MPa, with the hit rate steadily increasing throughout the 1 min of observation. (c and d) A 58 ms long snapshot of the continuous waveforms and (e and f) their spectrograms when the pore fluid is vented out by the solenoid valve for EB25 and EB175, respectively. In Figures 1c and 1d the thick black and green lines are top and bottom pore pressures, respectively, while the thin blue line represents the streaming data. In Figures 1e and 1f, red denotes the higher amplitudes in the signal at that particular frequency and time, while green/blue represents lower amplitudes. At 25°C (Figure 1e), a broadband tremor occurred, starting 12 ms after the release and lasting for 10 ms. At 175°C (Figure 1f) the tremor starts 5 ms after the release and has a duration of 30 ms, with the power of the signal concentrated at few discrete frequencies, 100 and 160 kHz.

To further investigate this frequency switch, a systematic statistical analysis was developed. This consisted of extracting a sequence of 819.2 µs long events from EB25 (56 events) and EB175 (31 events) in the 120 s following the venting. In each signal, the initial onset time was picked and a fast Fourier transform analysis was performed over a 102.4 µs long window in order to obtain a characteristic frequency of the AE. This permits the dominant frequency of each event to be superimposed on the pore pressure decay (Figures 2a and 2b). In general, we note that the dominant frequencies generated at 25°C fall within the frequency range 40–160 kHz (Figure 2a), whereas at 175°C two subtle ranges of dominant frequency emerge: 90–110 kHz and 160–180 kHz (Figure 2b). This analysis has been performed on the other five experiments, which resulted in analogous results (Figure S3).

To evaluate the extent of the broadband feature in EB25 and of the bimodality in EB175, we use a cross-correlation analysis on the event waveforms in each experiment. The method cross correlates the waveforms between events, resulting in a matrix of cross-correlation coefficients. Choosing a threshold of 0.7, we then define a master event, corresponding to the event with the highest number of correlated event. For each of the correlated events, a spectrum over the same time window of 102.4 µs has been calculated, and finally, these spectra are stacked, resulting in the plots shown in Figures 2c and 2d. In EB25, 15 events are correlated and the stacked spectrum has a broadband feature, with 9 of these events being classified as broadband. In EB175, 12 events are correlated, displaying a well-defined bimodality with narrower spectral peaks, with 7 of these events classified as bimodal.

Figures 3a and 3c show a spectral analysis of these waveforms for the two master spectra and their wave-forms occurring in EB25 and EB175. When the streaming data are harvested into discrete events, a range of broadband and bimodal features is observed during the tremor-like AE activity, depending on the P/T conditions. In EB25 the amplitude spectrum lies constantly above the −6 dB threshold from 80 to 145 kHz (Figure 3a). Conversely in EB175 only two narrow frequency ranges lie above the −6 dB threshold: 80–105 kHz and 150–180 kHz (Figure 3c).

Finally, AE focal mechanisms were calculated. Due to the low amplitude, low SNR, and low number of picks available (just eight channels recorded streaming data), reasonable focal mechanisms were obtained for only 11 AEs harvested during the venting stage of both experiments (six for EB25 and five for EB175: Table S1). These 11 events show a component of double couple (DC) (ranging from 7% to 60%, with an average of 32%). The component of compensated linear vector dipole is slightly higher, ranging from 21% to 61% and with an average of 42%, reflecting the enhanced contribution of the fluid motion to the mechanism [e.g., *Julian*, 1994; *Benson et al.*, 2008].

4. Discussion and Conclusions

During our experiments we recorded AE events in the frequency range from 40 to 200 kHz. This is comparable to the field-scale volcanic seismic signals occurring at frequencies 0.1–10 Hz via simple frequency/scale relationship [*Aki and Richards*, 1980; *Burlini et al.*, 2007; *Benson et al.*, 2008; *Browning et al.*, 2016]. LP and VLP signals with both unimodal and bimodal spectra have been observed at Mount Etna on 5 September 2013 (Figure 3b) and 10 January 2015 (Figure 3d) respectively (recorded by INGV permanent seismic array operating at Mount Etna). The 5 September VLP event is characterized by a spectrum, with a single peak, between 0.5 Hz and 2 Hz, lying above the −6 dB threshold and has been associated to the explosive activity at the New Southeast Crater, which involves gas-rich erupted magma [*Bonaccorso et al.*, 2014] and is typically accompanied by intense degassing at the nearby craters [*Viccaro et al.*, 2015].

The 10 January LP signal instead shows a spectrum with two peaks above the −6 dB line, at 4–5 Hz and at 7.5 Hz, and has been linked to strombolian activity and ash emission at Voragine crater. We therefore notice the link between a monophase fluid (gas) and a single-peak spectrum, while a double-phase fluid (liquid-gas) produces a two-peak spectrum. Bimodal spectra have also been found at Stromboli volcano [*Sgroi et al.*, 2009] and interpreted as the overlap of deep magmatic fluids and shallower fluids enriched of gas. This is consistent with our findings, confirming the key role played by the type and number of phases forming the fluid to the character of the fluid-induced seismicity. Although the comparison between fluid-induced AE and volcanic LP and VLP signals has been previously postulated by *Julian* [1994] and shown qualitatively in the laboratory by *Benson et al.* [2008], in this work we expand this to better analyze the competition between gas and liquid due to elevated temperatures and with respect to pore pressure decompression in order to understand the
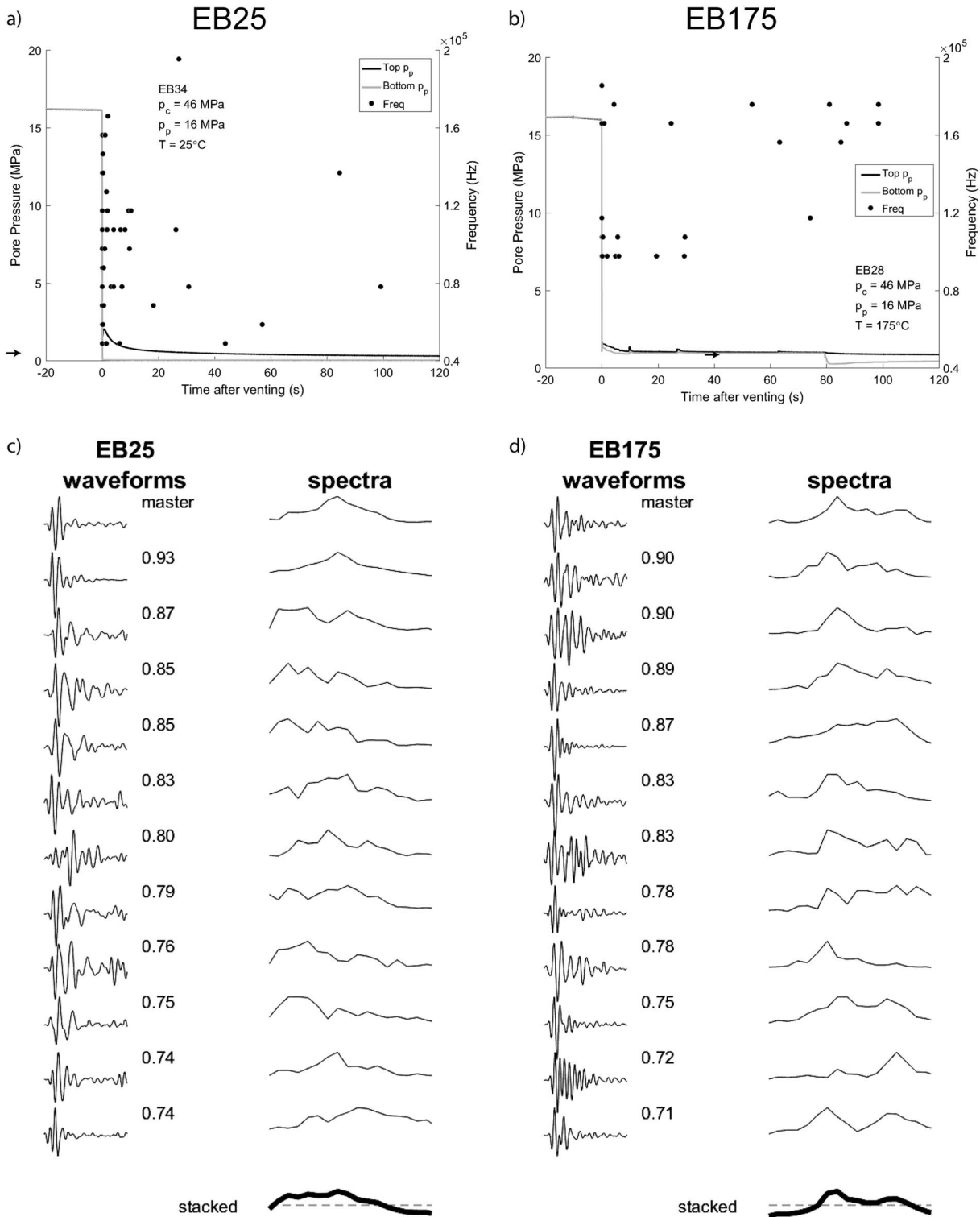
Figure 2. (a and b) The top (black) and bottom (grey) pore pressure-time plot (left hand axis, solid lines) with dominant event frequencies shown on the right-hand axis (black filled circles) of the harvested events for EB25 and EB175 experiments, respectively. The arrows indicated the events shown in detail in Figures 3a and 3c. (c and d) The correlated waveforms and their spectra. The number on the waveform is the correlation coefficient with the master waveform. On the bottom right of each panel, the spectra, resulting from the stacking of the spectra of the correlated events, are plotted, with the dashed horizontal line marking −6 dB level. While in EB25 a broadband spectrum characterizes the correlated events, the stacked spectrum in EB175 presents two peaks. These characteristics are similar to those observed for the tremors (Figures 2c and 2d), suggesting that the number of phases in the fluid controls the spectrum of the AE activity.
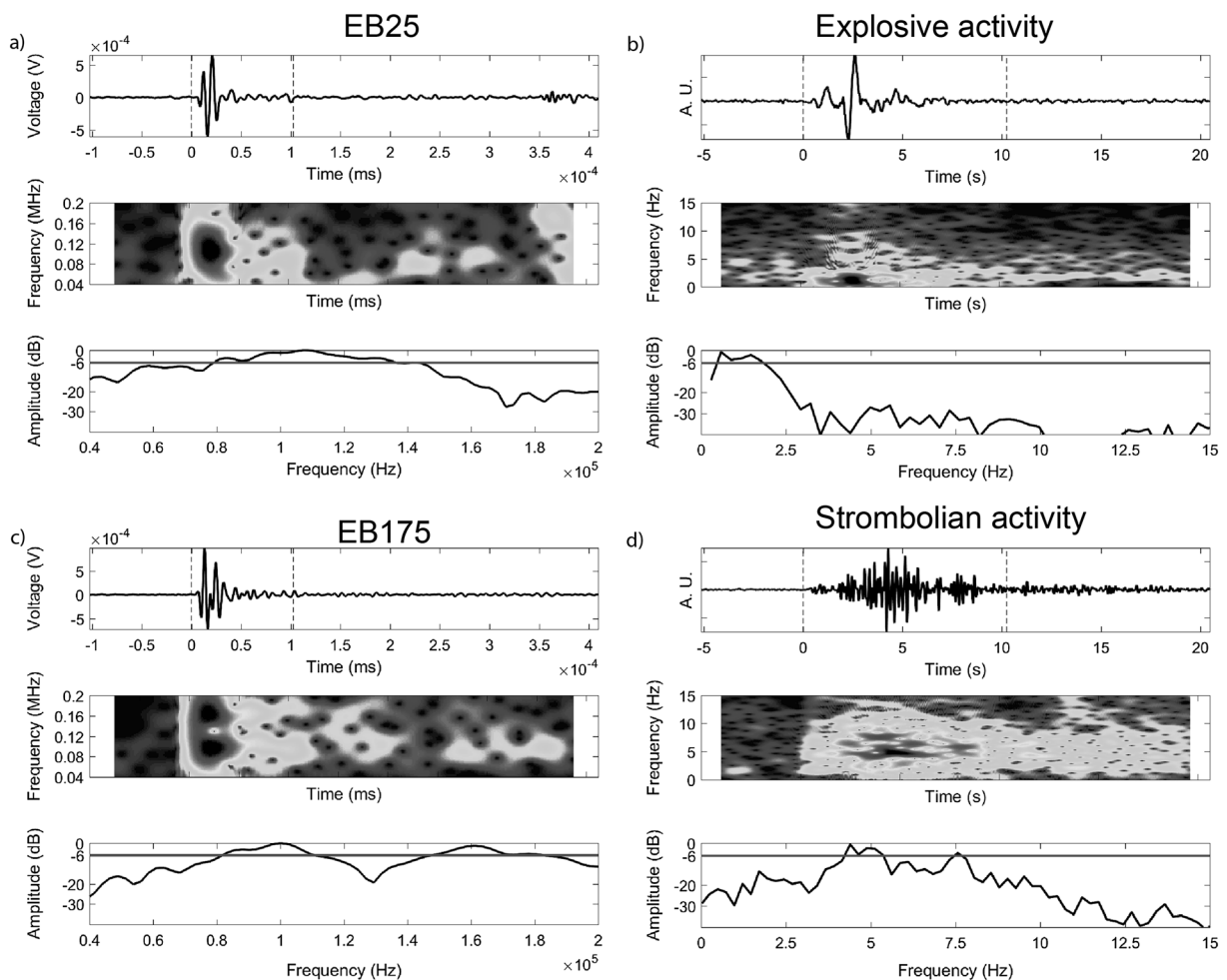
Figure 3. The laboratory signals of experiment (a) EB25 and (c) EB175 are matched with the (b and d) field-scale volcanic events. Each panel shows the waveforms (top part), the spectrogram (middle part), and the waveform spectral density (in dB units, bottom part). The fast Fourier transform is calculated from the onset of the event over a 1024-point long window (vertical dashed lines). At 25°C (Figure 3a), the event is characterized by a broadband spectrum with a frequency range of 80–145 kHz above the −6 dB threshold. This is somehow similar to the VLP event (Figure 3b) recorded at Mount Etna (Italy) on 5 September 2013, where a single peak (0.5–2 Hz) above the −6 dB is present. This volcanic signal was recorded 3 min before mild explosive activity at the New Southeast Crater. At 175°C two dominant frequency ranges appear above the −6 dB threshold: 80–105 kHz and 150–180 kHz (Figure 3c). A similar bimodality (first peak between 4.5 Hz and 5.5 Hz and second narrower peak at 7.5 Hz) has been observed in the LP event (Figure 3d) recorded at the same volcano on 10 January 2015. This LP signal was associated to the continuous strombolian activity and ash emission from the Voragine crater. This volcanic activity is marked by the simultaneous presence of both liquid and gas phases. Field-scale events come from INGV seismic network.

relationship between the source and the corresponding signal. This is important, as while the basic mechanism for AE generation due to the rapid movement of water through a fractured zone (as the pore pressure is released) is known, the precise role of the pore fluid phase (water, bubbly liquids, etc.) that generates turbulence manifested as a sustained tremor (Figures 1c and 1d) has yet to be constrained mainly due to the difficulties in generating low-amplitude events with acceptable quality and build a catalogue in meaningful statistical terms.

To better understand the interactions between the rock matrix (damage zones) and the influence of pore fluids and pressure fluctuations, we have developed a suite of experiments to cover a wide spectrum of fluid phases and consider the dominant frequency of events to better understand the contribution of the pore fluid water/gas phases to the generated AE and the distribution of these AEs across their dominant frequencies as a function of time and fluid pressure (Figures 2a and 2b). This is a key novelty with respect to previous early work that used the end-members given by either fully fluid saturated or dry rocks. For the events generated at 25°C, we obtained a fluid movement consisting of a single-phase liquid. Once the fluid is

released, a broadband tremor takes place followed by events with dominant frequencies widespread in the same frequency of the tremor, but characterized by a largely monochromatic spectrum, as shown in Figure 2 c. Conversely, at 175°C, well above the boiling temperature of water (at ambient pressure), a multiphase system is generated by the venting with a liquid-gas mixture being released to ambient pressure. These two phases coexisted inside the sample, due to the significant gradient in pore pressure between the upper and the lower ends of the sample, likely generating a time-varying "bubbly liquid"-type of fluid. We interpret the resulting bimodal AE event activity (with two clear dominant frequencies at 100 and 160 kHz) to be a consequence of a two-phase bubbly fluid. This has previously been established as the source of low-frequency activity, both in the laboratory and the field.

Quality factor (Q) analysis (Figure S4) revealed lower Q for experiment with liquid water and higher Q when a bubbly liquid is released, consistently with the model of *Kumagai and Chouet* [2000, 2001]. *Kumagai and Chouet* [2000, 2001] also postulated a higher-frequency content for fluids richer in gas, which explains the 160 kHz cluster toward the end of the venting stage (Figure 2b), where the gas fraction is expected to be higher due to the continued transformation of superheated water into gas. The decrease in the amplitude ratio between the spectral peak at 100 kHz and the spectral peak at 160 kHz (Figure S5) points to the same direction (additional discussion in the supporting information).

Examining the pore pressure curve in EB175 (Figure 1d), further evidence for the presence of a two-phase fluid stems from the plateauing of top and bottom pressures at approximately 1 MPa. This is close to the stable equilibrium condition where liquid water exists (approximately 0.7 MPa) at 175°C. The small discrepancy (0.3 MPa) is likely to be due to the time lag due to the placement of the measuring transducers, located about 2 m (top pressure) and 1.5 m (bottom pressure) away from the sample itself. Furthermore, the reexpansion of the fluid and the establishment of equilibrium is then likely to impede the pore pressure decay and therefore the generation of AEs. This is supported by the occurrence of only four events during the first seconds of release (Figure 1d), while some 27 events were recorded in the same time window for the venting at 25°C (Figure 1c). We also observed individual events of short duration (Figures 3a and 3c) that we interpret as fluid generated, due to the relatively low DC component (32%) and the similarity in the frequency content between these and their subsequent tremor. Both cases are consistent with a response to sudden pressure transient and sustained pressure fluctuations [e.g., *Chouet*, 1996].

The key findings of this study are (1) to find a better defined role of pore pressure decay rate on the generation of AEs and how these transition from sustained tremor of tens of milliseconds long to discrete events with similar spectral characteristics but hundreds of microseconds long and (2) the simulation and characterization of the role of phase changes in the pore fluid on the characteristic AE spectrum, determining subtle changes to the spectrogram depending on fluid phase mixture. Such an outcome has been theoretically postulated by *Kumagai and Chouet* [2000, 2001] who considered a range of different fluids within fracture damage zones such as dusty gasses and bubbly fluids resonating through different crack geometries. Taken together, our data provide new quantitative evidence for models linking low-frequency signals in volcanic areas as due to the resonance of high-pressure fluid-filled crack/cavities [e.g., *Chouet*, 1996]. We also suggest that low-frequency events (tremor, LPs, and VLPs) could be used to discriminate between different fluid-driven processes, ultimately helping eruption forecasting by characterizing the different supercritical fluids at depth and providing better constraints on the emplacement mechanics within the volcanic edifice generally [*Neuberg*, 2000]. We find that the effects of the fluids phase/type on the AE data (and by extension field seismic data) are very subtle, and so using such an analysis to infer deep magmatic plumbing systems should be done with caution.

References

Aki, K., and P. G. Richards (1980), *Quantitative seismology: Theory and methods*, vol. II, W.H. Freeman, San Francisco, Calif.

Alparone, S., A. Cannata, S. Gambino, S. Gresta, V. Milluzzo, and P. Montalto (2010), Time-space variation of volcano-seismic events at La Fossa (Vulcano, Aeolian Islands, Italy): New insights into seismic sources in a hydrothermal system, *Bull. Volcanol.*, 72(7), 803–816.

Benson, P. M., B. D. Thompson, P. G. Meredith, S. Vinciguerra, and R. P. Young (2007), Imaging slow failure in triaxially deformed Etna basalt using 3D acoustic-emission location and X-ray computed tomography, *Geophys. Res. Lett.*, 34, L03303, doi:10.1029/2006GL028721.

Benson, P. M., S. Vinciguerra, P. G. Meredith, and R. P. Young (2008), Laboratory simulation of volcano seismicity, *Science*, 322(5899), 249–252.

Benson, P. M., S. Vinciguerra, P. G. Meredith, and R. P. Young (2010), Spatio-temporal evolution of volcano seismicity: A laboratory study, *Earth Planet. Sci. Lett.*, 297(1), 315–323.

Benson, P. M., S. Vinciguerra, M. H. Nasseri, and R. P. Young (2014), Laboratory simulations of fluid/gas induced micro-earthquakes: Application to volcano seismology, *Front. Earth Sci.*, *2*, 32.

Bonaccorso, A., S. Calvari, A. Linde, and S. Sacks (2014), Eruptive processes leading to the most explosive lava fountain at Etna volcano: The 23 November 2013 episode, *Geophys. Res. Lett.*, *41*, 4912–4919, doi:10.1002/2014GL060623.

Browning, J., P. Meredith, and A. Gudmundsson (2016), Cooling-dominated cracking in thermally stressed volcanic rocks, *Geophys. Res. Lett.*, *43*, 8417–8425, doi:10.1002/2016GL070532.

Burlini, L., S. Vinciguerra, G. Di Toro, G. De Natale, P. Meredith, and J. P. Burg (2007), Seismicity preceding volcanic eruptions: New experimental insights, *Geology*, *35*(2), 183–186.

Chouet, B. (2003), Volcano seismology, *Pure Appl. Geophys.*, *160*(3–4), 739–788.

Chouet, B. A. (1996), Long-period volcano seismicity: Its source and use in eruption forecasting, *Nature*, *380*(6572), 309–316, doi:10.1038/380309a0.

Chouet, B. A., and R. S. Matoza (2013), A multi-decadal view of seismic methods for detecting precursors of magma movement and eruption, *J. Volcanol. Geotherm. Res.*, *252*, 108–175.

Iverson, R. M., et al. (2006), Dynamics of seismogenic volcanic extrusion at Mount St Helens in 2004–05, *Nature*, *444*(7118), 439–443.

Julian, B. R. (1994), Volcanic tremor: Non-linear excitation by fluid flow, *J. Geophys. Res.*, *99*, 11,859–11,877, doi:10.1029/93JB03129.

Kendrick, J. E., Y. Lavallée, T. Hirose, G. Di Toro, A. J. Hornby, S. De Angelis, and D. B. Dingwell (2014), Volcanic drumbeat seismicity caused by stick-slip motion and magmatic frictional melting, *Nat. Geosci.*, *7*(6), 438–442.

Kumagai, H., and B. A. Chouet (2000), Acoustic properties of a crack containing magmatic or hydrothermal fluids, *J. Geophys. Res.*, *105*, 25,493–25,512, doi:10.1029/2000JB900273.

Kumagai, H., and B. A. Chouet (2001), The dependence of acoustic properties of a crack on the resonance mode and geometry, *Geophys. Res. Lett.*, *28*, 3325–3328, doi:10.1029/2001GL013025.

McNutt, S. R. (1996), Seismic monitoring and eruption forecasting of volcanoes: A review of the state-of-the-art and case histories, in *Monitoring and Mitigation of Volcano Hazards*, pp. 99–146, Springer, Berlin.

McNutt, S. R. (2005), Volcanic seismology, *Ann. Rev. Earth planet. Sci.*, *32*, 461–491.

Nelder, J. A., and R. Mead (1965), A simplex method for function minimization, *Comput. J.*, *7*(4), 308–313.

Neuberg, J. (2000), Characteristics and causes of shallow seismicity in andesite volcanoes, *Philos. Trans. R. Soc. London*, *358*(1770), 1533–1546.

Neuberg, J. W., H. Tuffen, L. Collier, D. Green, T. Powell, and D. Dingwell (2006), The trigger mechanism of low-frequency earthquakes on Montserrat, *J. Volcanol. Geotherm. Res.*, *153*(1), 37–50.

Ohnaka, M., and K. Mogi (1982), Frequency characteristics of acoustic emission in rocks under uniaxial compression and its relation to the fracturing process to failure, *J. Geophys. Res.*, *87*, 3873–3884, doi:10.1029/JB087iB05p03873.

Pettitt, W. S. (1998), *Acoustic Emission Source Studies of Microcracking in Rock*, Doctoral dissertation, Univ. of Keele.

Press, W. H., B. P. Flannery, S. A. Teukolsky, and W. T. Vetterling (1994), *Numerical Recipes in C: The Art of Scientific Computing*, 2nd ed., Cambridge Univ. Press, Cambridge.

Read, M. D., M. R. Ayling, P. G. Meredith, and S. A. Murrell (1995), Microcracking during triaxial deformation of porous rocks monitored by changes in rock physical properties: II. Pore volumometry and acoustic emission measurements on water-saturated rocks, *Tectonophysics*, *245*(3), 223–235.

Saccorotti, G., I. Lokmer, C. J. Bean, G. Di Grazia, and D. Patanè (2007), Analysis of sustained long-period activity at Etna Volcano, Italy, *J. Volcanol. Geotherm. Res.*, *160*(3), 340–354.

Sammonds, P. R. (1999), Understanding the fundamental physics governing the evolution and dynamics of the Earth's crust and ice sheets, *Philos. Trans. R. Soc. London*, *357*(1763), 3377–3401.

Sgroi, T., C. Montuori, R. Agrusta, and P. Favali (2009), Low-frequency seismic signals recorded by OBS at Stromboli volcano (Southern Tyrrhenian Sea), *Geophys. Res. Lett.*, *36*, L04305, doi:10.1029/2008GL036477.

Tuffen, H., and D. Dingwell (2005), Fault textures in volcanic conduits: Evidence for seismic trigger mechanisms during silicic eruptions, *Bull. Volcanol.*, *67*(4), 370–387.

Viccaro, M., R. Calcagno, I. Garozzo, M. Giuffrida, and E. Nicotra (2015), Continuous magma recharge at Mt. Etna during the 2011–2013 period controls the style of volcanic activity and compositions of erupted lavas, *Mineral. Petrol.*, *109*(1), 67–83.